Eur. Phys. J. B **1**, 419–428 (1998)

THE EUROPEAN PHYSICAL JOURNAL B

Concerning the first-order phase transition in the low-dimensional organic superconductor $(BEDO-TTF)_2ReO_4 \cdot H_2O$. Crystal and electronic band structures below the phase transition (T = 170 K)

S.S. Khasanov[1], B.Zh. Narymbetov[1], L.V. Zorina[1], L.P. Rozenberg[1], R.P. Shibaeva[1,a], N.D. Kushch[2], E.B. Yagubskii[2,b], R. Rousseau[3], and E. Canadell[3,c]

[1] Institute of Solid State Physics, Russian Academy of Sciences, 142432 Chernogolovka, MD, Russia
[2] Institute of Chemical Physics in Chernogolovka, Russian Academy of Sciences, 142432 Chernogolovka, MD, Russia
[3] Institut de Ciencia de Materials de Barcelona (CSIC), Campus de la U.A.B., 08193 Bellaterra, Spain

Received: 4 September 1997 / Received in final form: 2 December 1997 / Accepted: 3 December 1997

Abstract. The effect of the first-order phase transition occurring around 220 K on the crystal and electronic structure of the molecular superconductor $(BEDO–TTF)_2ReO_4 \cdot H_2O$ has been studied. The crystal structure at 170 K has been determined and it is found that the main structural change resulting from the phase transition is connected with a rotation of the ReO_4^- anions. This rotation leads to changes in the S···S and S···O intermolecular contacts within the BEDO–TTF donor layers. How these structural changes affect the electronic structure of the salt is studied by comparing the transfer integrals for the different donor···donor intermolecular interactions calculated for the room temperature and 170 K crystal structures. It is shown that Fermi surfaces for the 170 K and room temperature structures are very similar, do not exhibit nesting properties, and can be described as resulting from the hybridization of superposing ellipses.

PACS. 61.66.Hq Organic compounds – 74.70.Kn Organic superconductors

1 Introduction

Most organic metals and superconductors known at present are cation-radical salts based on bis(ethylenedithio) tetrathiafulvalene, BEDT–TTF [1]. BEDO–TTF — bis-(ethylenedioxo) tetrathiafulvalene) — is a symmetric analog of BEDT–TTF, in which the four oxygen atoms replace the four sulfur atoms in the peripheral rings [2]. A number of BEDO–TTF salts with different anions like I_3^-, AuI_2^-, IBr_2^-, $Ag(CN)_2^-$, $CF_3SO_3^-$ and $Cu(NCS)_2^-$, has been synthesized and structurally characterized [3–15]. It is noteworthy that crystals of the BEDO–TTF cation-radical salts usually are not isostructural with crystals of the corresponding BEDT–TTF salts. Parenthetically, BEDO–TTF itself is not isostructural with BEDT–TTF. Many BEDO–TTF based organic metals have been prepared but only two of them $(BEDO–TTF)_3Cu_2(NCS)_3$ [6] and $(BEDO–TTF)_2ReO_4 \cdot H_2O$ [9,10] have been found to be superconductors. This is also in contrast with the fact that many BEDT–TTF based superconductors have been prepared.

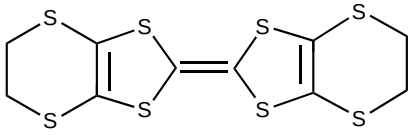

BEDT-TTF

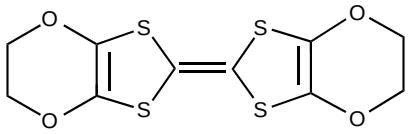

BEDO-TTF

$(BEDO–TTF)_2ReO_4 \cdot H_2O$ is of particular interest among the BEDO–TTF cation-radical salts because of the quite peculiar physical behavior it exhibits [9,10, 16–20]. It is a quasi-two-dimensional room temperature metal which undergoes several phase transitions as the temperature is lowered. The crystals exhibit metallic behavior down to ≈ 35 K. In the temperature interval from 220 to 205 K there is a drastic decrease of the resistance.

[a] e-mail: shibaeva@issp.ac.ru
[b] e-mail: yagubski@icp.ac.ru
[c] e-mail: canadell@zas.qf.ub.es

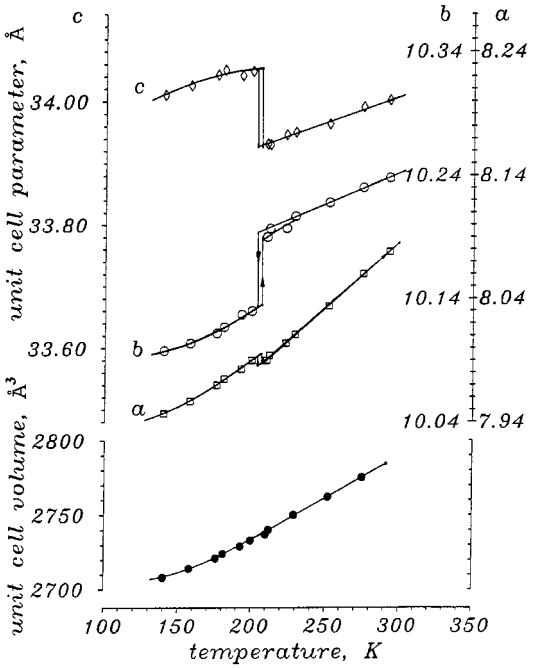

Fig. 1. The lattice constants and volume as a function of temperature for the (BEDO–TTF)$_2$ReO$_4 \cdot$ H$_2$O single crystals.

This anomaly is associated with a strong hysteresis [9,10] which points out to a first order metal-metal phase transformation. Another phase transition has been evidenced at 90 K by thermopower [9] and Electron-Spin Resonance (ESR) experiments [18]. Resistivity [9,10], Hall effect and ESR measurements [18] evidenced the existence of still another phase transition at $\sim$ 35 K, which has been proposed to originate from a spin density wave instability of the Fermi surface [10]. Finally, there is a superconducting transition with onset at 2.5-3.5 K [9,10].

The different physical measurements reported so far for (BEDO–TTF)$_2$ReO$_4 \cdot$ H$_2$O have not led to a completely satisfactory view of its electronic structure and the origin of the different phase transitions. This is (at least partially) due to the fact that a study of the evolution of the crystal structure as the temperature is lowered, *i.e.*, as one goes through the successive phase transitions, is not yet available. As a first step towards a more in-depth understanding of the physical behavior of this very interesting system we report here a study of its crystal and electronic structure at 170 K, *i.e.* after the first transition. This will provide us with a direct way to analyze the origin and consequences of the initial first-order phase transition. Among other things, this will also make possible the characterization of the Fermi surface after the crystal structure changes brought about by the first-order phase transition. This Fermi surface should be a better approximation to the low-temperature one and thus, it could maybe provide some clues to analyze the origin of the 35 K phase transition as well as the results of recent magnetoresistance studies.

Table 1. Main crystal data for (BEDO–TTF)$_2$ReO$_4 \cdot$ H$_2$O at 170 K and 293 K. $C_{20}H_{18}O_{13}S_8Re$, $F(000) = 1780$, $M = 909.0$, sp. gr. P $2_1/n$, $Z = 4$.

Parameter	170 K	293 K
a, Å	7.975(3)	8.072(3)
b, Å	10.117(4)	10.230(4)
c, Å	34.040(9)	34.012(9)
γ, °	97.28(3)	98.00(3)
V, Å^3	2724.3	2781.3
$d_{\mathrm{calc.}}$, g/cm^3	2.22	2.17
μ, cm^{-1}	51.4	50.3

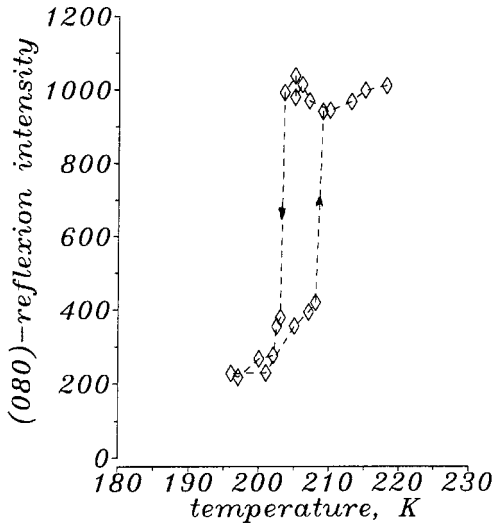

Fig. 2. Temperature dependence of the (080)-reflexion intensity.

2 X-ray study and crystal structure

The main crystal data for (BEDO–TTF)$_2$ReO$_4 \cdot$ H$_2$O at 170 K and room temperature [10,11] are collected in Table 1. The X-ray diffraction data were measured using an Enraf-Nonius CAD-4F diffractometer with graphite monochromated MoK$_\alpha$ radiation (λ = 0.71073 Å). The intensities of 3818 independent reflections with $I \geq 3\sigma(I)$ were collected by the ω scan method in the range $(\sin\Theta/\lambda)_{\max} = 0.628$ Å^{-1}. Intensities were corrected for Lorentz and polarization effects, but an absorption correction was not applied.

The variation of the unit cell parameters with temperature was measured from room temperature down to 140 K. The temperature dependence of the unit cell parameters is shown in Figure 1. As can be seen from this figure all unit cell parameters are decreasing normally from 293 to 203 K, but there is a sharp decrease of the b-parameter and a sharp increase of the c-parameter at the point of the phase transition. As a result, the temperature dependence of the unit cell volume exhibits a normal behavior without any discontinuity around 203 K. However, the

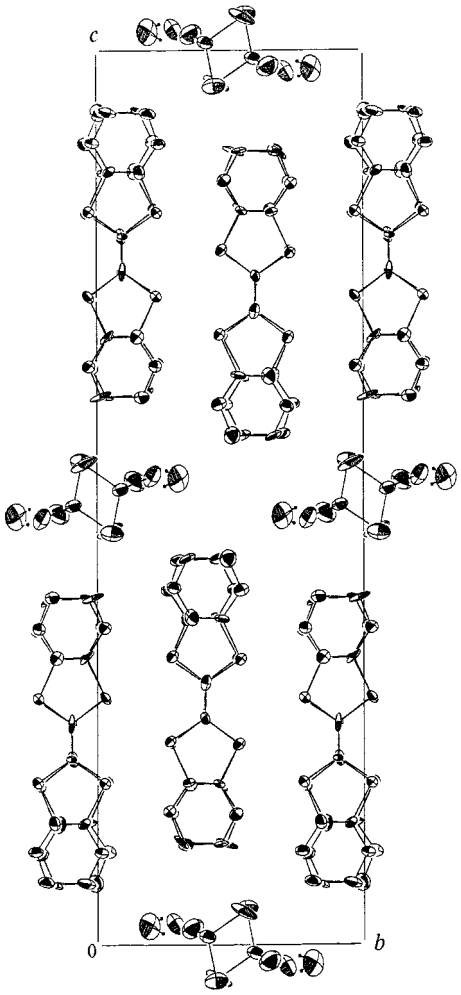

Fig. 3. Projection of the crystal structure of (BEDO–TTF)$_2$ReO$_4 \cdot$ H$_2$O viewed along the a-axis.

effect of the first-order phase transition in the (BEDO–TTF)$_2$ReO$_4 \cdot$ H$_2$O single crystals is also reflected in the temperature dependence of the (080)-reflection intensity (Fig. 2).

The structure was solved by a direct method using the AREN programs [21] and then refined by an anisotropic least-square method (isotropic for H) using the SHELXL programs [22] to $R = 0.063$ for 3350 reflections with $F \geq 4\sigma(F)$. The final coordinates and equivalent isotropic thermal parameters of the nonhydrogen atoms are listed in Table 2 and those for the hydrogen atoms in Table 3. Figure 3 represents the projection of the crystal structure along the a-direction. From the crystallographical viewpoint, the first-order phase transition is mainly characterized by changes in the anion layer but without any drastic modification of the basic crystal structure. Nevertheless, the changes in the anion layer affect the inner structure of the conducting BEDO–TTF layers. So it is very important to carefully compare the structures above and below the phase transition temperature.

Table 2. Atomic coordinates and equivalent isotropic thermal parameters $U_{\rm eq}$ (Å^2) for the non hydrogen atoms of (BEDO–TTF)$_2$ReO$_4 \cdot$ H$_2$O at 170 K.

Atom	x/a	y/b	z/c	$U_{\rm eq}$(*)
S1	0.6047(6)	0.0288(4)	0.1806(1)	0.017(1)
S2	0.3751(6)	−0.2258(4)	0.1816(1)	0.018(1)
S3	0.3714(6)	−0.2232(4)	0.2749(1)	0.016(1)
S4	0.5998(6)	0.0312(4)	0.2752(1)	0.018(1)
O1	0.613(2)	0.015(1)	0.1028(3)	0.023(3)
O2	0.389(2)	−0.233(1)	0.1043(4)	0.020(3)
O3	0.367(1)	−0.220(1)	0.3529(3)	0.020(3)
O4	0.593(2)	0.029(1)	0.3534(3)	0.023(3)
C1	0.490(2)	−0.098(1)	0.2079(5)	0.015(4)
C2	0.551(2)	−0.049(2)	0.1356(5)	0.018(4)
C3	0.525(3)	−0.042(2)	0.0687(5)	0.033(5)
C4	0.499(2)	−0.194(2)	0.0705(5)	0.026(4)
C5	0.446(2)	−0.162(2)	0.1364(5)	0.020(4)
C6	0.488(2)	−0.097(1)	0.2474(6)	0.022(4)
C7	0.429(2)	−0.152(2)	0.3202(5)	0.019(4)
C8	0.454(3)	−0.170(2)	0.3881(5)	0.025(4)
C9	0.488(3)	−0.015(2)	0.3873(5)	0.027(5)
C10	0.536(2)	−0.039(2)	0.3205(5)	0.020(4)
S5	0.1124(6)	0.0380(4)	0.1820(1)	0.018(1)
S6	−0.1159(6)	−0.2177(4)	0.1786(1)	0.019(1)
S7	−0.1291(6)	−0.2257(4)	0.2726(1)	0.016(1)
S8	0.0974(6)	0.0305(4)	0.2761(1)	0.017(1)
O5	0.126(2)	0.040(1)	0.1040(4)	0.027(3)
O6	−0.094(2)	−0.212(1)	0.1011(4)	0.024(3)
O7	−0.136(2)	−0.230(1)	0.3507(3)	0.021(3)
O8	0.085(2)	0.020(1)	0.3543(3)	0.021(3)
C11	−0.007(2)	−0.092(1)	0.2079(5)	0.017(4)
C12	0.063(2)	−0.031(2)	0.1363(5)	0.018(4)
C13	0.037(3)	−0.008(2)	0.0688(6)	0.031(5)
C14	0.006(3)	−0.161(2)	0.0682(5)	0.031(5)
C15	−0.043(2)	−0.144(2)	0.1350(6)	0.025(4)
C16	−0.011(2)	−0.095(1)	0.2474(5)	0.018(4)
C17	−0.075(2)	−0.157(2)	0.3187(5)	0.020(4)
C18	−0.041(3)	−0.186(2)	0.3853(5)	0.026(4)
C19	−0.012(2)	−0.036(2)	0.3877(5)	0.021(4)
C20	0.027(2)	−0.044(2)	0.3202(5)	0.016(4)
Re	0.2520(1)	0.4114(1)	0.0089(0)	0.024(0)
O9	0.447(2)	0.356(2)	0.0180(5)	0.051(4)
O10	0.084(2)	0.292(1)	0.0235(4)	0.043(4)
O11	0.232(2)	0.443(1)	−0.0401(4)	0.037(4)
O12	0.241(2)	0.548(2)	0.0370(4)	0.055(5)
O$_{\rm w}$	0.734(2)	0.193(2)	0.0206(7)	0.061(5)

(*) $U_{\rm eq}$ is defined as one third of the trace of the orthogonalized $U_{\rm eq}$ tensor.

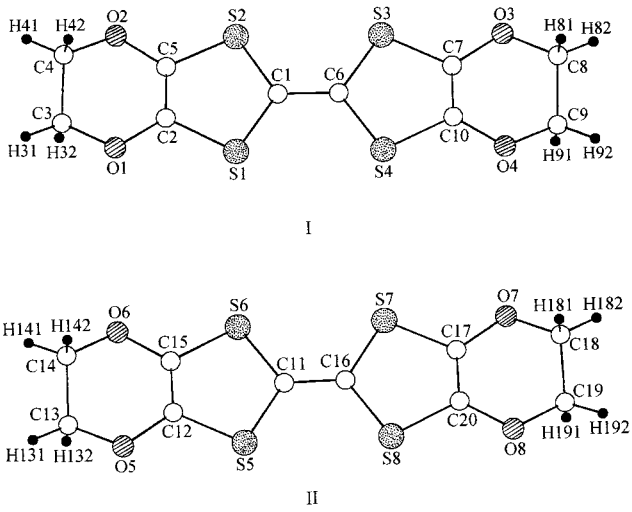

Fig. 4. Atomic numbering for the BEDO–TTF cation-radicals I and II in $(BEDO–TTF)_2ReO_4 \cdot H_2O$.

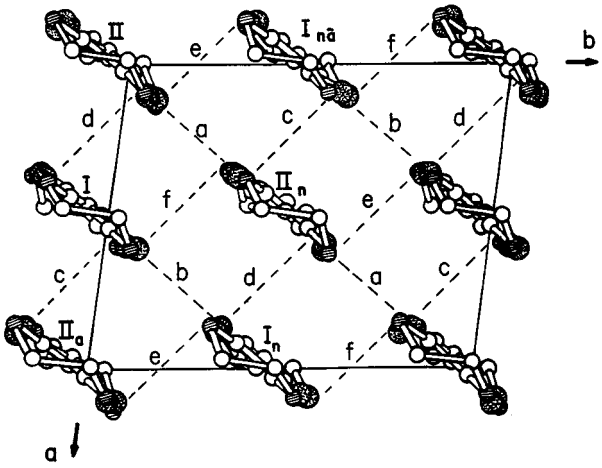

Fig. 5. Projection of the cation-radical layer along *c*.

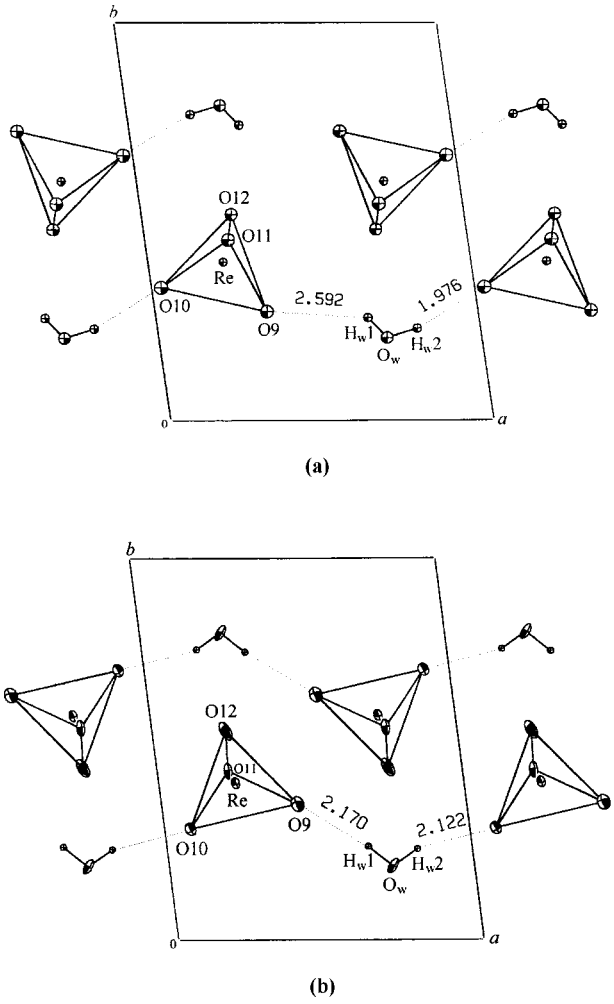

Fig. 6. Projection of the anion layer on the *ab* plane for: (a) $T = 293$ K and (b) $T = 170$ K.

The crystal structure consists of cation-radical layers parallel to the *ab*-plane, alternating with layers of the ReO_4^- anions and H_2O molecules. There are two crystallographically nonequivalent cation radicals of BEDO–TTF, I and II, which occupy general positions. The atomic numbering of these cation-radicals is shown in Figure 4. The cation-radical layers (Fig. 5) are build from BEDO–TTF stacks parallel to *a*. The cation-radical stacks can be considered to be regular both at room temperature and 170 K. The bond length and angles are such that the BEDO–TTF molecules I and II can be considered as identical. They both have the same eclipsed conformation of terminal ethylene groups. The ethylene groups in I and II are ordered at both temperatures. The two independent cation-radicals remain nearly parallel (the angle between the planes of the molecules I and II is 0.8° at 293 K and 0.6° at 170 K).

The two crystallographically independent interplanar distances I–II and I–II_a are equal within experimental error (3.49(4) Å at 293 K) and they become a little bit smaller (3.43(5) Å) at 170 K. The overlap modes of neighboring cation-radicals in a stack are the same at both temperatures. The cation-radical layer contains a large number of short S$\cdots$S and S$\cdots$O contacts. Those shorter than the sum of the van der Waals radii, as well as the corresponding ones at room temperature, are listed in Table 4. It should be noted that the four last contacts given in this table are intrastack ones, whereas all other are interstack side-by-side contacts. It is also worth noting that although many of these contacts are shorter at 170 K, this is not the case for all of them.

Projections of the anion layer on the *ab*-plane are shown in Figure 6. At room temperature (see Fig. 6a) the ReO_4^- anions are bonded to the water molecules through hydrogen bonding. The strongest one is associated with a distance $H_w2\cdots O10a$ of 1.98 Å, an angle O_w-H_w2-$O10a$ of 162° and an $O_w\cdots O10a$ distance of 2.75 Å. The next closest distance from H_2O to ReO_4^- is $H_w1\cdots O9$ 2.59 Å. The O_w-H_w1-O9 angle is 126° and the $O_w\cdots O9$ distance is 3.09 Å. Thus, although the water molecules bridge two

Table 3. Atomic coordinates for the hydrogen atoms of $(BEDO–TTF)_2ReO_4 \cdot H_2O$ at 170 K.

Atom	x/a	y/b	z/c
H31	0.589(3)	−0.014(2)	0.0453(5)
H32	0.416(3)	−0.010(2)	0.0669(5)
H41	0.446(2)	−0.230(2)	0.0465(5)
H42	0.606(2)	−0.227(2)	0.0736(5)
H81	0.561(3)	−0.206(2)	0.3902(5)
H82	0.387(3)	−0.198(2)	0.4110(5)
H91	0.381(3)	0.021(2)	0.3857(5)
H92	0.545(3)	0.017(2)	0.4113(5)
H131	0.104(3)	0.023(2)	0.0459(6)
H132	−0.070(3)	0.027(2)	0.0673(6)
H141	−0.051(3)	−0.191(2)	0.0441(5)
H142	0.113(3)	−0.196(2)	0.0688(5)
H181	0.067(3)	−0.221(2)	0.3847(5)
H182	−0.101(3)	−0.222(2)	0.4085(5)
H191	−0.120(2)	−0.001(2)	0.3883(5)
H192	0.048(2)	−0.009(2)	0.4118(5)
H_w1	0.661(20)	0.245(18)	0.012(7)
H_w2	0.820(17)	0.239(4)	0.029(9)

ReO_4^- units in the anionic chain running along a, they really form an hydrogen bond with only one anion. A rather different picture of the anion layer at 170 K can be seen in Figure 6b. It is evident that the first-order phase transition at 203 K is accompanied by a reorientation of the ReO_4^- anions. Now the position of the H_2O molecule is more symmetrical. The distances $O_w \cdots O10a$ and $O_w \cdots O9$ are 2.84 and 2.98 Å, respectively, while the distances $H_w2 \cdots O10a$ and $H_w1 \cdots O9$ are 2.12 and 2.17 Å, respectively. The angles O_w-H_w2-O10a and O_w-H_w1-O9 become 147° and 155°, respectively. It should be noted that some deformation of the ReO_4^- anion itself occurs when lowering the temperature: two bond angles, O9-Re-O10 and O9-Re-O12, increase by $\sim 5°$ when compared with the room temperature values, while the remaining tetrahedral angles practically do not change.

Thus the X-ray structural study of the single crystals of $(BEDO–TTF)_2ReO_4 \cdot H_2O$ below the first-order phase transition reveals that this transition is connected with changes in the anion layer. A reorientation of the ReO_4^- anions at 203 K causes the jumps of the unit cell parameters c and b in opposite directions: the b-parameter decreases but the c-parameter increases. Then, the crystal system relaxes when lowering the temperature (see Fig. 1) but nevertheless the parameter c at $T = 170$ K remains larger than its room temperature value. Of course, the change in the anion layer has an effect on the interactions between the anion and cationic layers. Shown in Table 5 are some intermolecular $O \cdots H$ contacts between the ReO_4^- anions and H_2O molecules with the BEDO–TTF donors. It is through such interlayer hydrogen bonding interactions, that the reorientation of the ReO_4^- anions affect the intermolecular BEDO–TTF $\cdots$ BEDO–TTF interactions in the donor layers and consequently, can lead to changes in their band structure and Fermi surface.

3 Electronic structure

3.1 Computational details

Our tight-binding band structure calculations are based upon the effective one-electron Hamiltonian of the extended Hückel method [23]. The off-diagonal matrix elements of the Hamiltonian were calculated according to the modified Wolfsberg-Helmholz formula [24]. All valence electrons were explicitly taken into account in the calculations and the basis set consisted of double-ζ Slater-type orbitals for C, S and O and single-ζ Slater type orbitals for H. The exponents, contraction coefficients and atomic parameters for C, S and H were taken from previous work [25]. The exponents (ζ_μ and $\zeta_{\mu'}$), contraction coefficients (c_μ and $c_{\mu'}$) and atomic parameters ($H_{\mu\mu}$) used for O were: 2.688, 1.675, 0.6739, 0.3567 and −32.3 eV for O 2s, and 3.694, 1.659, 0.3322, 0.7448 and −14.8 eV for O 2p.

3.2 Band structure and Fermi surface

The calculated band structure for the BEDO–TTF slabs of the 170 K structure of $(BEDO–TTF)_2ReO_4 \cdot H_2O$ is shown in Figure 7a. Since our main purpose here is to analyze the effect of the first-order phase transition on the electronic structure of $(BEDO–TTF)_2ReO_4 \cdot H_2O$, we also report in Figure 8a the calculated band structure for the room temperature structure using exactly the same computational details. The unit cell of the BEDO–TTF slabs contains four donor molecules, two of which are symmetry inequivalent. Thus, the band structures of Figures 7a and 8a contain four HOMO bands. With the average oxidation state of $(BEDO–TTF)^{+1/2}$ there are six electrons to fill these bands. Since the third and fourth bands from the bottom overlap, $(BEDO–TTF)_2ReO_4 \cdot H_2O$ should exhibit a metallic behavior, as experimentally found, and the Fermi surface should possess both electron and hole pockets. The calculated Fermi surfaces for the 170 K and room temperature structures are shown in Figures 7b and 8b, respectively.

Let us first consider the results for the 170 K structure. The calculated band structure (see Fig. 7a) is characterized by a noticeable band dispersion for the upper two bands along both the a^* (see $\Gamma \rightarrow$ X) and b^* (see $\Gamma \rightarrow$ Y) directions which suggests a two-dimensional nature of the electronic structure around the Fermi level. The two doubly degenerate levels at the special points X and Y are the result of band sticking due to the n-glide symmetry operation running parallel to the $a+b$ direction. Near the special point X, the third band from the bottom crosses the Fermi level creating a hole pocket around this point (see Fig. 7b). The area of this pocket is 4.9% of the first

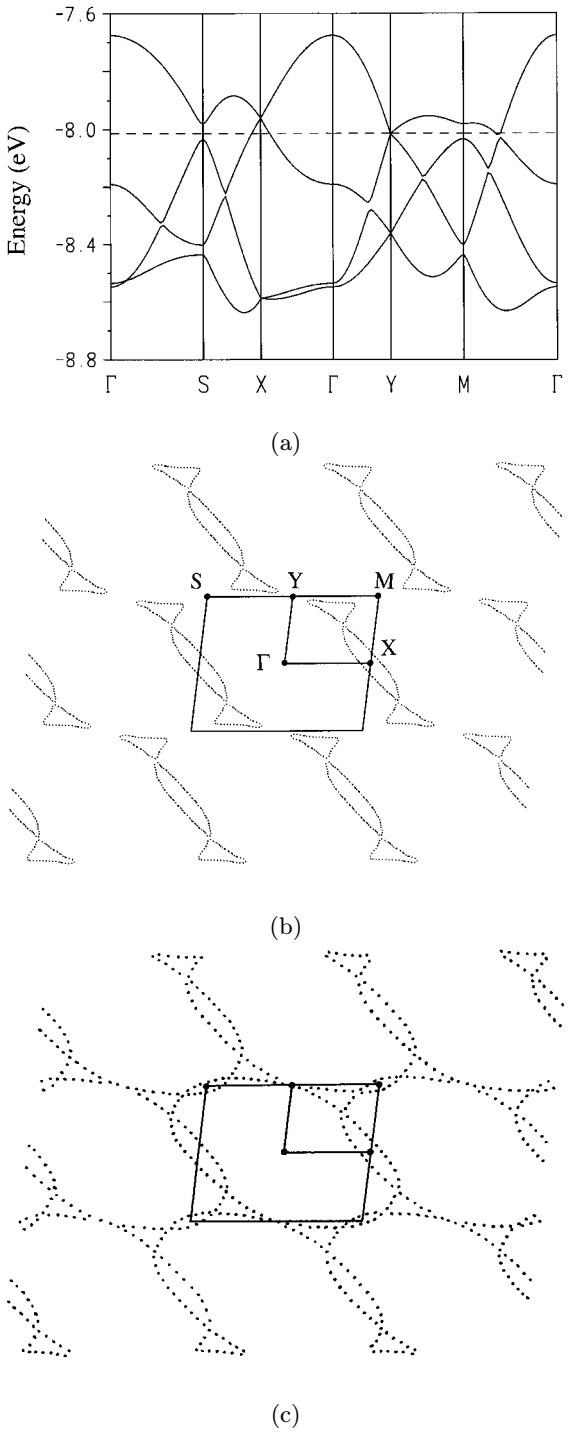

Fig. 7. Calculated dispersion relations (a) and Fermi surface (b) for the HOMO bands of the 170 K crystal structure of (BEDO–TTF)$_2$ReO$_4 \cdot$ H$_2$O. The dashed line in (a) indicates the Fermi level. Γ, X, Y, M and S refer to the wave vectors (0, 0), ($a^*/2$, 0), (0, $b^*/2$), ($a^*/2$, $b^*/2$) and ($-a^*/2$, $b^*/2$), respectively. Shown in (c) is a schematic drawing suggesting that the Fermi surface in (b) can be seen as resulting from a series of superposing ellipses.

Brillouin zone. Two identical and symmetry related electron pockets arising from the fourth band appear inside the Brillouin zone away from any of the directions chosen in the dispersion diagram. The area of each of these pockets is 2.45% of the first Brillouin zone. It is worth mentioning that the calculated Fermi level lands almost directly on the doubly degenerate level at point Y. Because of this fact, extremely small changes in the Fermi level can induce either a small electron or hole pocket at Y. In fact the two electron pockets near Y may collapse into a single electron pocket by extremely small changes in the transfer integrals. What these results highlight is that the Fermi surface around Y (*i.e.*, the electron pockets) can be easily and considerably modified. This could be at the origin of some of the puzzling magnetoresistance results reported for (BEDO–TTF)$_2$ReO$_4 \cdot$ H$_2$O [20,26] since very minor geometrical changes brought about either by thermal contraction or pressure, could significantly modify the shape of the Fermi surface around Y [27]. A strong magnetic field [26] could probably also induce noticeable changes in this region. Anyway, what it is already clear from even a quick look at Figure 7b, is that the 170 K Fermi surface of (BEDO–TTF)$_2$ReO$_4 \cdot$ H$_2$O can be seen as resulting from the weak hybridization of superposed ellipsoid Fermi surfaces (see Figs. 7b and 7c). In other words, (BEDO–TTF)$_2$ReO$_4 \cdot$ H$_2$O at 170 K should be a quite 2D metal.

Let us now compare the band structure and Fermi surface of the 170 K (Fig. 7) and room temperature (Fig. 8) structures. There is a surprising similarity between the two figures especially if one considers that there is a first-order phase transition between the two structures. The main difference is that the area of the Fermi surface slightly increases from room temperature to 170 K. The area of the hole pocket increases from 3.7% of the first Brillouin zone to 4.9% when going from room temperature to 170 K. However, in almost any respect the room temperature Fermi surface is practically identical to the 170 K one. Thus, (BEDO–TTF)$_2$ReO$_4 \cdot$ H$_2$O should be considered as a 2D conductor with Fermi surface resulting from a series of superposing ellipses. In fact this is even more clear in the 170 K Fermi surface (see Fig. 7b) because of the slight changes in the region of the electron pockets. These results cast serious doubts on the previous interpretation of the 35 K resistivity anomaly as arising from nesting of two "hidden" 1D Fermi surfaces [18]. The shape of the hole pocket in the present and previous [18] studies are very similar (note that the previous study used a different set of crystal axes). The difference between the two studies lies in the shape of the two symmetry related electron pockets. As noted above, the nature of the band structure is such that the shape of these electron pockets can be quite sensitive to the location of the Fermi level and/or to details of the computations, like the size of the k-points mesh used to sample the Brillouin zone. We have verified that our computed Fermi surface is converged with respect to the size of the k-points mesh [28]. Since otherwise the computational details for the two studies are the same we think that the Fermi surfaces of Figures 7b

Table 4. Short S$\cdots$S ($r \leq 3.70$ Å) and S$\cdots$O ($r \leq 3.35$ Å) contacts between the BEDO–TTF cation-radicals.

Contact	r, Å		BEDO–TTF (*)	Donor$\cdots$Donor Interaction Type
	170 K	293 K		
S1$\cdots$S3 (S3$\cdots$S1)	3.430	3.539	$I–I_{n}$ ($I–I_{n\bar{a}\bar{b}}$)	b
S1$\cdots$S7 (S7$\cdots$S1)	3.655	3.722	$I–II_{n}$ ($II–I_{n\bar{a}\bar{b}}$)	f
S2$\cdots$S4 (S4$\cdots$S2)	3.413	3.346	$I–I_{n\bar{a}\bar{b}}$ ($I–I_{n}$)	b
S2$\cdots$S8 (S8$\cdots$S2)	3.522	3.609	$I–II_{n\bar{b}}$ ($II–I_{n\bar{a}}$)	e
S3$\cdots$S4 (S4$\cdots$S3)	3.523	3.564	$I–I_{n\bar{a}\bar{b}}$ ($I–I_{n}$)	b
S3$\cdots$S5 (S5$\cdots$S3)	3.586	3.624	$I–II_{n\bar{b}}$ ($II–I_{n\bar{a}}$)	e
S3$\cdots$S8 (S8$\cdots$S3)	3.689	3.763	$I–II_{n\bar{b}}$ ($II–I_{n\bar{a}}$)	e
S4$\cdots$S6 (S6$\cdots$S4)	3.603	3.725	$I–II_{n}$ ($II–I_{n\bar{a}\bar{b}}$)	f
S4$\cdots$S7 (S7$\cdots$S4)	3.630	3.661	$I–II_{n}$ ($II–I_{n\bar{a}\bar{b}}$)	f
S5$\cdots$S7 (S7$\cdots$S5)	3.331	3.394	$II–II_{n}$ ($II–II_{n\bar{a}\bar{b}}$)	a
S6$\cdots$S8 (S8$\cdots$S6)	3.551	3.593	$II–II_{n\bar{a}\bar{b}}$ ($II–II_{n}$)	a
S7$\cdots$S8 (S8$\cdots$S7)	3.497	3.486	$II–II_{n\bar{a}\bar{b}}$ ($II–II_{n}$)	a
S1$\cdots$O3 (O3$\cdots$S1)	3.282	3.506	$I–I_{n}$ ($I–I_{n\bar{a}\bar{b}}$)	b
S2$\cdots$O4 (O4$\cdots$S2)	3.349	3.208	$I–I_{n\bar{a}\bar{b}}$ ($I–I_{n}$)	b
S5$\cdots$O7 (O7$\cdots$S5)	3.097	3.152	$II–II_{n}$ ($II–II_{n\bar{a}\bar{b}}$)	a
S1$\cdots$S6 (S6$\cdots$S1)	3.549	3.573	$I–II_{a}$ ($II–I_{\bar{a}}$)	c
S2$\cdots$S5 (S5$\cdots$S2)	3.596	3.645	I–II (II–I)	d
S3$\cdots$S8 (S8$\cdots$S3)	3.575	3.610	I–II (II–I)	d
S4$\cdots$S7 (S7$\cdots$S4)	3.587	3.646	$I–II_{a}$ ($II–I_{\bar{a}}$)	c

(*) Symmetry codes:
I, II (x, y, z); $I_{\bar{a}}$ $(x-1, y, z)$; II_{a} $(x+1, y, z)$; I_{n}, II_{n} $(1/2+x, 1/2+y, 1/2-z)$;
$I_{n\bar{a}}$ $(x-1/2, 1/2+y, 1/2-z)$; $II_{n\bar{b}}$ $(1/2+x, y-1/2, 1/2-z)$;
$I_{n\bar{a}\bar{b}}$, $II_{n\bar{a}\bar{b}}$ $(x-1/2, y-1/2, 1/2-z)$.

and 8b are more reliable. Recently, Horiuchi *et al.* [29] also reported a Fermi surface for the room temperature structure of $(BEDO–TTF)_2ReO_4 \cdot H_2O$ which, although marginally different in details, is also consistent with our view of an hybridization of overlapping ellipses. This view does not only account for the fact that the Fermi surface of Figure 7b does not exhibit nesting properties, but strongly suggests that in the absence of noticeable structural changes this should also be the case at lower temperatures. We thus believe that the 35 K resistivity anomaly does not originate from a nesting mechanism.

Table 5. Comparison of some O$\cdots$H intermolecular contacts between the anion or H_2O and the BEDO–TTF donors.

Contact	r, Å		BEDO–TTF (*)
	170 K	293 K	
O11$\cdots$H192	2.43	2.29	II_{in}
O12$\cdots$H92	2.35	2.53	$I_{n\bar{a}}$
$O_w\cdots$H31	2.42	2.53	I
$O_w\cdots$H41	2.75	2.42	I_{ia}

(*) Symmetry codes:
I_{ia} $(1-x, -y, -z)$, II_{in} $(1/2-x, 1/2-y, z-1/2)$

3.3 Effect of the first-order transition on the transfer integrals

To understand the link between the structural changes induced in the donor layers by the reorientation of the ReO_4^- anions and the apparent lack of effect on the electronic structure, we must consider in detail the different donor$\cdots$donor intermolecular interactions in the BEDO–TTF layers. As shown in Figure 5, there are six different types of BEDO–TTF$\cdots$BEDO–TTF intermolecular interactions. The associated transfer integrals for the 170 K and room temperature crystal structures calculated according to the usual dimer splitting approximation [30] are reported in Table 6. It is worth noting that the difference in HOMO energies of the BEDO–TTF donors I and II is only 0.078 eV at room temperature and 0.028 eV at 170 K. Thus, although the two independent donors are quite similar even at room temperature, they become even more so after the first-order phase transition.

Three different classes of HOMO$\cdots$HOMO interactions can be distinguished in the BEDO–TTF slabs. Interactions a and b are of the side-by-side type and

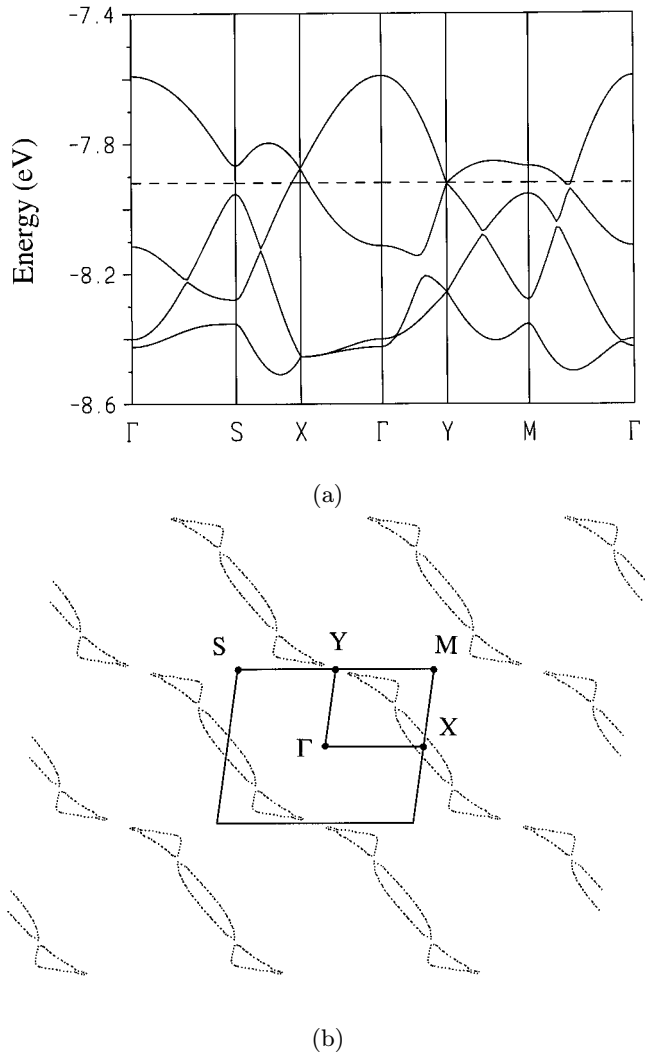

Fig. 8. Calculated dispersion relations (a) and Fermi surface (b) for the HOMO bands of the room temperature crystal structure of $(BEDO–TTF)_2ReO_4 \cdot H_2O$. The dashed line in (a) indicates the Fermi level. Γ, X, Y, M and S refer to the wave vectors (0, 0), ($a^*/2$, 0), (0, $b^*/2$), ($a^*/2$, $b^*/2$) and ($-a^*/2$, $b^*/2$), respectively.

provide for chains of molecules running along the $(a+b)$-direction. Interaction a runs between type-II molecules and interaction b between type-I molecules. We note that these interactions are larger than similar interactions in BEDT–TTF based salts. However, they are not the largest interactions in the slab. According only to the S$\cdots$S distances, these interactions should be by far the stronger interactions of the slab. They are not because of the side-by-side arrangement which leads to a relatively weak π-type overlap between the adjacent HOMOs. Interactions c and d run parallel to the a-direction leading to chains of the form $\cdot\cdot$I$\cdot\cdot$c$\cdot\cdot$II$\cdot\cdot$d$\cdot\cdot$I$\cdot\cdot$c$\cdot\cdot\cdot$. These interactions although clearly smaller are far from being negligible. The third class is that of interactions e and f. These interactions run along the b-direction leading to step-chains along that direction. As found in many BEDT–TTF salts

Table 6. Comparison of the $t_{HOMO-HOMO}$ transfer integrals (eV) calculated for the 170 K and room temperature structures of $(BEDO–TTF)_2ReO_4 \cdot H_2O$.

Intermolecular interaction	$t_{HOMO-HOMO}$ (eV)	
	170 K	293 K
a	−0.126	−0.121
b	−0.127	−0.125
c	−0.064	−0.064
d	−0.044	−0.061
e	0.170	0.163
f	0.163	0.147

these interactions are the largest. Since none of the interactions of the three different types of chains along the a-, b- and $(a+b)$-directions is negligible, the quite isotropic 2D metallic character of this salt is not difficult to understand. As far as the HOMO$\cdots$HOMO interactions are concerned, the donor slabs of $(BEDO–TTF)_2ReO_4 \cdot H_2O$ can be described as a series of strongly interacting parallel donor step-chains.

The discussion of the previous paragraph equally applies to the room temperature and 170 K structures. If we now compare the two sets of transfer integrals in Table 6, it is clear that the overall difference is essentially quite small. This fact alone accounts for the very small changes in the band structure and Fermi surface before and after the transition. The more significant differences in the transfer integrals are those of interactions d and f. It is interesting to look now again at the data in Table 4. If one should pinpoint what interaction is more strongly affected by the first-order transition according to the changes in the S$\cdots$S and S$\cdots$O distances, interaction b would be chosen. However, according to the transfer integrals of Table 6 there is practically no change in the corresponding HOMO$\cdots$HOMO interaction. This apparent contradiction is however not so difficult to understand. To begin with, some of the changes run in opposite directions. When taking this into account it is clear that the overall change in the S$\cdots$S interactions is not very large. The changes in the S$\cdots$O distances (−0.224 Å and +0.141 Å) are the largest in the donor slabs. Even if having opposite signs, an important effect in the associated transfer integral could be expected. However it must be pointed out that the contribution of the oxygen p orbitals to the HOMO of BEDO–TTF is quite small. In fact it is even smaller than that of the sulfur p orbitals on the same positions of BEDT–TTF, where this contribution was only one-third of that of the inner sulfur p orbitals. Thus the a and b transfer integrals are quite insensitive to the changes in the S$\cdots$O distances.

It is clear that it is only the variation on the S$\cdots$S short contacts that should be considered when comparing the effect of the first-order transition on the transfer integrals. The largest shortening when going from room temperature to 170 K occurs for interaction f. This interaction, the largest in the slab, is of the strong σ-type and

consequently, it is understandable that the largest shortening in the S···S distances leads to the largest change in the transfer integrals. We note that the changes in the S···S distances of interaction e, which is of the same type, are smaller but however non negligible. Indeed the change in the transfer integral is about half that of interaction f. Thus, most of the changes in the transfer integrals of Table 6 are not that difficult to understand, even if they are not very large, once the nature of the BEDO–TTF HOMO and the changes in the S···S distances are taken into account. The only puzzling variation is that of interaction d. The changes in the associated S···S distances, like those of interaction c, are among the smaller ones. Yet whereas the transfer integral for *c* remains unaltered, that for d experiences a variation comparable to that of interaction f. This is a reminder that, because of the strong directional character of the HOMO, distances alone can not lead to a complete understanding of the strength of the intermolecular interactions. The slight sliding motion of one of the two donors of interaction d with respect to the other leads, even without major changes in the S···S contacts, to a decrease in the absolute value of the transfer integral. Such decrease is in itself small but in the context of the present discussion it is a significant one. The decrease in the absolute value of the transfer integral d is apparently nearly compensated by the increase in the absolute value of the transfer integral f, leaving the electronic structure almost unchanged.

At this point it is clear that the changes in the transfer integrals do not lead to strong modifications in the electronic structure of $(BEDO–TTF)_2ReO_4 \cdot H_2O$ as it goes through the first- order phase transition. Why should then the resistivity exhibit a jump at the corresponding temperature? Our discussion in Section 2 clearly shows that there is a reorientation of the ReO_4^- anions and the water molecules during the phase transition. Thus, the outer coulombic field felt by the conducting electrons before and after the transition is certainly different and this presumably leads to the resistivity jump.

4 Concluding remarks and prospect for future studies

As a result of the present study it may be concluded that the first-order phase transition in $(BEDO–TTF)_2ReO_4 \cdot H_2O$ at 203 K involves rather essential changes on the anion layer which however do not strongly affect the Fermi surface. This does not mean that the changes in the anion layer are not transmitted to the donor layer. Indeed there are quite significant changes in both the S···O and S···S short contacts. However comparison of the crystal structures at room temperature and 170 K shows that the short S···S distances, except for those of the side-by-side interactions, behave "normally", *i.e.*, they shorten as the temperature is lowered. In contrast, the short S···O and S···S distances of the side-by-side interactions behave in a different way: some become shorter ($I–I_n$ 3.506 → 3.282 Å and 3.539 → 3.430 Å), and some become longer ($I–I_n$, $I–I_{nab}$ 3.208 → 3.349 Å and 3.346 → 3.413 Å). These are among the largest relative changes in the donor slabs and those which are mainly brought about by the changes in the anion layer. In principle, it could be expected that the transfer integrals associated with these interactions would be those showing the larger changes as a result of the first-order transition. However the π-type nature of these HOMO···HOMO interactions and the weak participation of the oxygen p orbitals into the HOMO lead to very small changes in these interactions. As a consequence, the first-order transition has only a minor effect on the band structure and Fermi surface of $(BEDO–TTF)_2ReO_4 \cdot H_2O$.

The previous observation leads to one of the more interesting aspects of the present study. As we have shown, the Fermi surface seems to be quite easily amenable to significant modifications around the region of the Y point. This suggests that the shape of the electron pockets can be seriously modified by small changes in the inner structure of the donor layers (*i.e.*, small changes in the transfer integrals). Consequently, it is quite remarkable that the Fermi surface remains practically unaltered when the system undergoes a first-order phase transition. This means that the changes in the transfer integrals responsible for the above mentioned changes of the Fermi surface in the region around Y are not those which are brought about by the first-order phase transition. The possibility that some of the puzzling results of recent magnetoresistance studies [20,26,31] can be related to the instability of the Fermi surface in the region around Y with respect to the small geometric changes brought about by thermal contraction and/or pressure, or even to strong magnetic fields, is thus an open question. Fermi surface simulations in order to establish the relationship between this instability and the relative values of the different transfer integrals, as well as X-ray studies of the crystal structure at temperatures lower than 170 K, are clearly needed.

The present study does not support the idea of a nesting mechanism leading to the formation of a spin density wave as a likely origin for the 35 K anomaly. However, since according to our results, the Fermi surface can be easily and seriously modified in some parts of the Brillouin zone, it is not possible to completely rule out that changes brought about by thermal contraction can lead to at least some partial nesting. Determination of the crystal structure near 35 K, in order to recalculate the Fermi surface, is crucially needed in order to unravel the origin of the resistivity anomaly at this temperature. Although the rationalization of the low temperature behavior of $(BEDO–TTF)_2ReO_4 \cdot H_2O$ still seems to be an elusive goal the present work suggests some directions worth following.

We are indebted to V.N. Laukhin for fruitful discussions of our results. This study was financially supported by the INTAS Grant 93-2400, the RFBR (Russian Foundation for Basic Researches) Grant 96-03-32029 and the DGES (Spain) Project PB96-0859.

References

1. J.M. Williams, J.R. Ferraro, R.J. Thorn, K.D. Carlson, U. Geiser, H.H. Wang, A.M. Kini, M.-H. Whangbo, *Organic Superconductors (including Fullerenes). Synthesis, Structure, Properties and Theory* (New Jersey: Prentice Hall, 1992).
2. T. Suzuki, H. Yamochi, G. Srdanov, K. Hincelman, F. Wudl, J. Am. Chem. Soc. **111**, 3108 (1989).
3. F. Wudl, H. Yamochi, T. Suzuki, H. Isotalo, C. Fite, K. Liou, H. Kasmai, G. Srdanov, in *The Physics and Chemistry of Organic Superconductors*, edited by G. Saito and S. Kagoshima (Springer-Verlag, Berlin, 1990), p. 358.
4. M.A. Beno, A.M. Kini, U. Geiser, H.H. Wang, K.D. Carlson, J.M. Williams, *The Physics and Chemistry of Organic Superconductors*, edited by G. Saito and S. Kagoshima (Springer Verlag, Berlin, 1990), p. 369.
5. M.A. Beno, H.H. Wang, K.D. Carlson, A.M. Kini, G.M. Frankenbach, J.R. Ferraro, N. Larson, G.D. McCabe, J. Thompson, C. Purnama, M. Vashon, J.M. Williams, Mol. Cryst. Liq. Cryst. **181**, 145 (1990).
6. M.A. Beno, H.H. Wang, A.M. Kini, K.D. Carlson, U. Geiser, W.K. Kwok, J.E. Thompson, J.M. Williams, Inorg. Chem. **29**, 1599 (1990).
7. H. Yamochi, T. Nakamura, G. Saito, T. Kikuchi, S. Sato, K. Nozawa, M. Kinoshita, T. Sugano, F. Wudl, Synth. Met. **42**, 1741 (1991).
8. T. Suzuki, H. Yamochi, H. Isotalo, C. Fite, H. Kasmai, K. Liou, G. Srdanov, F. Wudl, P. Coppens, K. Maly, A. Frost-Jensen, Synth. Met. **41-43**, 2225 (1991).
9. S. Kahlich, D. Schweitzer, I. Heinen, S.E. Lan, B. Nuber, H.J. Keller, K. Winzer, H.W. Helberg, Solid State Commun. **8**, 191 (1991).
10. L.I. Buravov, A.G. Khomenko, N.D. Kushch, V.N. Laukhin, A.I. Schegolev, E.B. Yagubskii, L.P. Rozenberg, R.P. Shibaeva, J. Phys. I. France **2**, 529 (1992).
11. R.P. Shibaeva, V.E. Zavodnik, Crystallogr. Rep. **38**, 195 (1993).
12. M. Fettouhi, L. Ouahab, D. Serhani, J.-M. Fabre, L. Ducasse, J. Amiell, R. Canet, P. Delhaes, J. Mater. Chem. **3**, 1101 (1993).
13. R. Li, V. Petricek, I. Cisarova, P. Coppens, Acta Cryst. **B51**, 798 (1995).
14. D. Schweitzer, S. Kahlich, I. Heinen, S.E. Lan, B. Nuber, H.J. Keller, K. Winzer, H.W. Helberg, Synth. Met. **55-57**, 2827 (1993).
15. T. Mori, K. Oshima, H. Okuno, H. Mori, S. Tanaka, Phys. Rev. B **51**, 11110 (1995).
16. S. Kahlich, D. Schweitzer, P. Auban-Senzier, D. Jérome, H.J. Keller, Solid State Commun. **83**, 77 (1992).
17. S. Kahlich, D. Schweitzer, P. Auban-Senzier, D. Jérome, H.J. Keller, Synth. Met. **56**, 2483 (1993).
18. S. Kahlich, D. Schweitzer, C. Rovira, J.A. Paradis, M.-H. Whangbo, I. Heinen, H.J. Keller, B. Nuber, P. Bele, H. Brunner, R.P. Shibaeva, Z. Phys. B **94**, 39 (1994).
19. A.E. Kovalev, S.I. Pesotskii, A. Gilevskii, N.D. Kushch, JETP Lett. **59**, 560 (1994); Pis'ma Zh. Eksp. Teor. Fiz. **59**, 530 (1994).
20. A. Audouard, P. Auban-Senzier, V.N. Laukhin, L. Brossard, D. Jérome, N.D. Kushch, Europhys. Lett. **34**, 599 (1996).
21. V.I. Andrianov, Kristallografiya **32**, 228 (1987).
22. G.M. Sheldrick, SHELXL-93, Program for refinement of crystal structures, University of Gottingen, Germany, 1993.
23. M.-H. Whangbo, R. Hoffmann, J. Am. Chem. Soc. **100**, 6093 (1978).
24. J. Ammeter, H.-B. Bürgi, J. Thibeault, R. Hoffmann, J. Am. Chem. Soc. **100**, 3686 (1978).
25. A. Pénicaud, K. Boubekeur, P. Batail, E. Canadell, P. Auban-Senzier, D. Jérome, J. Am. Chem. Soc. **115**, 4101 (1993).
26. A. Audouard, V.N. Laukhin, C. Proust, L. Brossard, N.D. Kushch, J. Phys. I France **7**, 599 (1997).
27. A detailed simulation study in which the role of the different transfer integrals in determining the shape of the Fermi surface is considered, is now underway. Preliminary results confirm the strong instability of the Fermi surface around the Y point. In contrast the Fermi surface around X is very stable, the only changes being the slight readjustment of the total area imposed by the reorganization around Y (R. Rousseau, E. Canadell, R.P. Shibaeva, work in progress).
28. In fact, the previously proposed Fermi surface can be generated when using sets of k-points smaller than those used in the present study.
29. S. Horiuchi, H. Yamochi, G. Saito, K. Sakaguchi, M. Kusunoki, J. Am. Chem. Soc. **118**, 8604 (1996).
30. P.M. Grant, J. Phys. Colloq. France **44**, C3-847 (1983).
31. V.N. Laukhin, personal communication.